UC San Diego

UC San Diego Previously Published Works

Title

Effects of deuteration on solid-state NMR spectra of single peptide crystals and oriented protein samples

Permalink

https://escholarship.org/uc/item/8b90h4mx

Authors

Long, Zheng
Park, Sang Ho
Opella, Stanley J

Publication Date

2019-12-01

DOI

10.1016/j.jmr.2019.106613

Peer reviewed

Effects of deuteration on solid-state NMR spectra of single peptide crystals and oriented protein samples

Zheng Long, **Sang Ho Park**, **Stanley J. Opella**[*]

Department of Chemistry and Biochemistry, University of California, San Diego, La Jolla, CA 92093-0309, United States

Abstract

Extensive deuteration can be used to simplify NMR spectra by "diluting" and minimizing the effects of the abundant ^{1}H nuclei. In solution-state NMR and magic angle spinning solid-state NMR of proteins, perdeuteration has been widely applied and its effects are well understood. Oriented sample solid-state NMR of proteins, however, is at a much earlier stage of development. In spite of the promise of the approach, the effects of sample deuteration are largely unknown. Here we map out the effects of perdeuteration on solid-state NMR spectra of aligned samples by closely examining differences in results obtained on fully protiated and perdeuterated samples, where all of the carbon sites have either ^{1}H or ^{2}H bonded to them, respectively. The ^{2}H and ^{15}N labeled samples are back-exchanged in ^{1}H$_2$O solution so that the amide ^{15}N sites have a bonded ^{1}H. Line-widths in the ^{15}N chemical shift, ^{1}H chemical shift, and ^{1}H-^{15}N dipolar coupling frequency dimensions were compared for peptide single crystals as well as membrane proteins aligned along with the phospholipids in bilayers with their normals perpendicular to the direction of the magnetic field. Remarkably, line-width differences were not found between fully protiated and perdeuterated samples. However, in the absence of effective ^{1}H-^{1}H homonuclear decoupling, the line-widths in the ^{1}H-^{15}N heteronuclear dipolar coupling frequency dimension were greatly narrowed in the perdeuterated samples. In proton-driven spin diffusion (PDSD) experiments, no effects of perdeuteration were observed. In contrast, in mismatched Hartmann-Hahn experiments, perdeuteration enhances cross-peak intensities by allowing more efficient spin-exchange with less polarization transfer back to the carbon-bound ^{1}H. Here we show that in oriented sample solid-state NMR, the effects of perdeuteration can be exploited in experiments where ^{1}H-^{1}H homonuclear decoupling cannot be applied. These data also provide evidence for the possible contribution of direct ^{15}N-^{15}N dilute-spin mixing mechanism in proton-driven spin diffusion experiments.

Keywords

Oriented sample solid-state NMR; Perdeuteration; ^{2}H decoupling; Triple-resonance; Spin-dilution; Spin-exchange; Protein NMR

[*]Corresponding author.: sopella@ucsd.edu (S.J. Opella).

1. Introduction

Dilution of ^{1}H nuclei through perdeuteration of nearby carbon sites with retention of a limited number of ^{1}H nuclei on specific carbon or nitrogen sites is a frequently used technique in protein NMR spectroscopy. In samples for solution-state NMR [1,2] and magic angle spinning solid-state NMR [3–5], substantial line narrowing results. Originally implemented to assist with resonance assignments and improve resolution, it is now most widely employed to narrow resonances through attenuation of strong [1]H-^{1}H homonuclear dipole-dipole interactions that affect relaxation in solution and line shapes in solid-state samples where local or global molecular motions are absent or insufficient to average out dipolar interactions.

In solid-state NMR, dilution of ^{1}H nuclei by deuteration of surrounding sites was first examined in nematic liquid crystals [6,7] and ice [8]; in both cases, ^{2}H decoupling was required in order to obtain high resolution ^{1}H NMR spectra. In addition to chemical dilution by replacement of the bulk of ^{1}H by ^{2}H, homonuclear [1]H-^{1}H dipolar interactions can be attenuated through the application of spectroscopic techniques, such as Lee-Goldburg (LG) continuous "magic-angle" irradiation [9], frequency-switched Lee-Goldburg (FSLG) [10], multiple pulse sequences, such as WAHUHA [11] and "magic sandwiches" [12]. Importantly, suppression of homonuclear dipolar interaction terms in the Hamiltonian through isotopic dilution or radiofrequency irradiations allows other interactions, such as chemical shifts and heteronuclear dipolar couplings, to be measured. Heteronuclear dipolar couplings provide information about chemical structures through measurements of internuclear distances and the angles between internuclear vectors and the magnetic field in stationary single crystal and uniaxially oriented samples. The heteronuclear dipolar couplings can be measured with separated local field (SLF) experiments [13,14]. Narrower line-widths and higher resolution are available through the implementation of FSLG [15] and magic-sandwich pulses [16,17] that suppress homonuclear 1H-^{1}H couplings.

Here we examine the role of perdeuteration in improving the measurement of heteronuclear dipolar couplings in peptides and proteins by utilizing the well-established model systems of single crystals of N-acetylated leucine (NAL) and the membrane-bound form of Pf1 coat protein in magnetically aligned phospholipid bilayers. The single amide site in each of the four NAL molecules in the crystal unit cell results in four signals with distinct ^{15}N chemical shift frequencies and [1]H-^{15}N heteronuclear dipolar coupling frequencies. Protein-containing bicelles align with their bilayer normals perpendicular to the direction of the magnetic field [18,19]. Since the protein molecules undergo rapid rotational diffusion about the bilayer normal, each ^{15}N backbone amide site yields a single-line resonance and a [1]H –[15]N dipolar coupling doublet that can be resolved in two-dimensional experiments.

Spin-exchange experiments rely on the presence of homonuclear dipole-dipole interactions between proximate nuclei to provide cross-peaks correlating pairs of nearby nuclei: a well-known example is the proton-driven spin diffusion (PDSD) experiment [20–22]. Perdeuteration of NAL with back-exchange of the amide ^{1}H drastically reduces the number of 1H available for spin-exchange. There are two ^{1}H and one ^{15}N in each NAL molecule following synthesis with deuterated reagents and subsequent ^{1}H back-exchange; by contrast,

without perdeuteration there are a total of fifteen ^{1}H and one ^{15}N in each NAL molecule. Direct comparisons of the results obtained from single crystals of these two samples demonstrate the effects of spin-dilution on the PDSD experiment. Similar comparisons can be made for the mismatched Hartmann-Hahn (MMHH) experiment [23] where irradiation at both ^{1}H and ^{15}N resonance frequencies effect ^{15}N-^{15}N spin-exchange through relays among ^{1}H nuclei [24]. This mechanism, which depends on intermediate ^{1}H spins between a pair of lower gamma spins undergoing exchange, is in contrast to the PDSD experiment where direct mixing occurs. The dilution of ^{1}H nuclei through replacement of many ^{1}H by ^{2}H and the implementation of homonuclear ^{1}H-^{1}H decoupling schemes have profound effects on the results of commonly used solid-state NMR experiments, such as resonance line-widths and intensities of spin-exchange cross-peaks.

2.   Experimental

2.1.   Sample preparation

Single crystals of NAL were prepared as described previously [25]. 100 mg of ^{15}N labeled L-leucine powder obtained from Cambridge Isotope Laboratories (www.isotope.com) was dissolved in 4 mL of warm glacial acetic acid and reacted with 0.8 mL of acetic anhydride. After solvent removal with a stream of nitrogen gas, the product was dissolved in 10 mL of warm high-performance liquid chromatography (HPLC) grade water and then lyophilized. 5 mL of a water–acetone mixture (1:1, v/v) was subsequently used to dissolve the synthesized N-Acetyl-L-Leucine (NAL). The solution was then passed through a 0.22 lm polyvinylidene fluoride syringe filter (www.emdmillipore.com). It was incubated for 4–10 days at room temperature until multiple 2–20 mg crystals could be harvested. Perdeuterated crystals were prepared following the same procedure except for the substitution of deuterated L-leucine and deuterated acetic anhydride, also obtained from Cambridge Isotope Laboratories, in the synthesis. The final crystallization step was carried out in a water-acetone solution at least four times in order to achieve complete ^{1}H back-exchange. Crystals with the "best" appearance were selected from the solution. An 8 mg ^{15}N labeled NAL single crystal and a 6 mg perdeuterated ^{15}N labeled NAL single crystal were used for the NMR experiments; they are referred to as the "protiated NAL" single crystal and the "perdeuterated NAL" single crystal, respectively.

Pf1 bacteriophage was prepared and purified as described previously [26]. Highly deuterated (>90%) and uniformly ^{15}N-labeled Pf1 bacteriophage were obtained by infecting *Pseudomonas aeruginosa* in Bioexpress cell growth media (U-^{2}H, 98%; U-^{15}N, 98%) and deuterium oxide (^{2}H, 99.9%) (www.isotope.com) [27]. The amide nitrogen sites were fully back-exchanged with ^{1}H by incubating the bacteriophage particles in ^{1}H$_2$O solution at 60 °C and pH 8 for 30 min, and then slowly cooling the solution to room temperature [28]. Pf1 coat protein-containing bicelles were prepared as described previously [19]. Here 2 mg of Pf1 coat protein was reconstituted in 25 mg of 1, 2-dimyristoyl-*sn*-glycero-3-phosphocholine (DMPC, www.anatrace.com) and mixed with a solution containing the detergent Triton X-100 (www.sigmaaldrich.com). The molar ratio (q) of DMPC to Triton X-100 was 5; and the DMPC concentration was 25% (w/v) in a total volume of 100 μL of 20 mM HEPES buffer at pH 6.7. For oriented sample solid-state NMR experiments, a flat-

bottomed 15 mm long NMR tube with 4 mm OD (newera-spectro.com) was filled with approximately 90 μL of the protein-containing bicelle solution.

2.2. HDN triple resonance probe

Two HDN triple-resonance probes were built for the solid-state NMR experiments. The probe circuit diagrams are shown in Fig. 1; the X channel represents the ^{2}H resonance frequency and the Y channel represents the ^{15}N resonance frequency. The probe associated with the circuit shown in Fig. 1A has a single solenoid coil (L1) triple-tuned to the ^{1}H, ^{2}H, and ^{15}N resonance frequencies corresponding to a ^{1}H resonance frequency of 700 MHz; the 8-turn solenoid coil has a 3.2 mm inner diameter and an 8 mm length. C2, C3, C9, C10, C12, and C13 are variable capacitors (NMNT10–6ENL from Voltronics Corp., www.dovermpg.com). C5 is a fixed chip capacitor (700C from ATC Corp., www.atceramics.com) and its value is selected to isolate the ^{2}H and ^{15}N channels. L3 and C7 constitute a band-stop filter at the ^{2}H resonance frequency. C6 and L2 provide a band-stop filter for the ^{1}H channel.

The circuit shown in Fig. 1B uses a cross-coil configuration: an outside loop-gap resonator (L1) is tuned for a ^{1}H resonance frequency of 900 MHz, and an inner solenoid coil (L3) is double-tuned for ^{2}H and ^{15}N resonance frequencies [29]. The loop-gap resonator (L1) has an inner dimension of 8.2 mm (width) by 7.75 mm (height) by 11.0 mm (length). The solenoid coil is an 8-turn 4 mm inner diameter coil with 0.25 mm thick Teflon coating. C3, C7, C13, C14, C17, and C18 are Voltronics variable capacitors (NMNT10–6ENL). C9, L2, and C11, L4 are two pairs of band-stop filters tuned to the ^{1}H channel: they are required to minimize the residual coupling between the loop-gap resonator and the solenoid coil. C8 is a fixed capacitor chosen to isolate the ^{15}N channel from the ^{2}H channel. L5 and C15 constitute a band-stop filter that isolates the ^{2}H channel from the ^{15}N channel. The fixed capacitor values and the probe performance measurements are in Table 1.

2.3. NMR experiments

Timing diagrams of the pulse sequences used to obtain the experimental data are shown in Fig. 2. ^{2}H decoupling was used for the deuterated samples; the timing of the ^{2}H decoupling pulse can be found on the last block of each individual pulse sequence.

Separated local field (SLF) (Fig. 2A) spectra for the NAL single crystal samples were acquired at a ^{1}H resonance frequency of 700 MHz with a 3 msec cross-polarization (CP) interval, 55 kHz ^{1}H B$_1$, 8 scans per t$_1$ value, and 10 msec acquisition times. Recycle delays of 4 sec and 20 sec were used for the protiated and perdeuterated NAL crystals, respectively. The dwell time for the indirect dimension was 20 μsec with 48 t$_1$ and 80 t$_1$ increments for the protiated and perdeuterated crystals, respectively. SPINAL-16 [30] decoupling was applied on the ^{1}H and ^{2}H channels following dipolar evolution with 70 kHz and 20 kHz power levels, respectively. SLF spectra for the magnetically oriented Pf1 coat protein bicelle samples were acquired at a 900 MHz ^{1}H frequency, using a 1 msec CP interval, 40 kHz ^{1}H B$_1$, 64 scans per t$_1$ and 10 msec acquisition time at 40 °C, with the exception of the experiment shown in Fig. 3, which had a 20 msec acquisition time. A recycle delay of 6 sec was used for both samples. Spectra for the Pf1 coat protein samples were acquired with a 40

kHz ^{1}H B$_1$. The dwell time for the indirect dimension was 20 μsec with 64 t$_1$ and 128 t$_1$ increments for the protiated and perdeuterated samples, respectively. SPINAL-16 decoupling was applied during signal acquisition, with 40 kHz and 10 kHz power levels on the ^{1}H and ^{2}H channels, respectively.

CP buildup experiments (Fig. 2B) used a dwell time of 10 μsec for the NAL crystal during t$_1$, and 20 μsec for the Pf1 coat protein samples. Spectra from SAMPI4 experiments (Fig. 2C) were acquired with a 70 kHz power level for both ^{1}H and ^{15}N B$_1$ for the NAL crystal samples and 35 kHz for the Pf1 coat protein samples. SPINAL-16 deuterium decoupling was applied during signal acquisition using a 20 kHz B$_1$ power level for the perdeuterated NAL, and a 10 kHz B$_1$ for perdeuterated Pf1 coat protein. The ^{2}H quadrupole echo experiments were performed with 55 kHz SPINAL-16 ^{1}H decoupling. The recycle delay of 16 sec maximized the intensity of the signals within ±20 kHz and ±60 kHz.

The heteronuclear correlation experiments (Fig. 2D) utilized SAMPI4 selective polarization transfer [31]. SPINAL-16 decoupling for the perdeuterated sample was applied during t$_1$ and t$_2$ on the ^{2}H channel. Spectra from both protiated and perdeuterated NAL single crystals were acquired with 4 scans for each of 256 t$_1$ increments at 70 kHz ^{1}H B$_1$ for SAMPI4 CP transfer, and decoupling during t$_1$ and t$_2$ intervals. The HETCOR spectrum for the protiated NAL crystal was acquired using 4 SAMPI4 dwells for selective polarization transfer. The HETCOR spectrum for the perdeuterated NAL was acquired with 3 SAMPI4 dwells, and a ^{2}H decoupling power of 35 kHz. Spectra for the Pf1 coat protein samples were acquired with 35 kHz ^{1}H B$_1$ for SAMPI4 CP transfer, and decoupling during t$_2$ intervals, and 43 kHz decoupling during t$_1$ intervals. Spectra for both protiated and perdeuterated Pf1 coat protein samples were acquired with 16 scans, 8 SAMPI4 dwells for selective polarization transfer, 6 sec recycle delay, 128 t$_1$ increments, and 5 msec acquisition time. 25 kHz and 10 kHz SPINAL-16 for ^{1}H and ^{2}H decoupling were used, respectively.

Spectra for PDSD experiments (Fig. 2E) were acquired with 55 kHz ^{1}H B$_1$ and ^{15}N B$_1$ fields, for 32 scans, 128 t$_1$ points and 100 μsec dwell times in the indirect dimension. For the perdeuterated NAL sample, ^{2}H decoupling with SPINAL-16 at 20 kHz was applied during t$_1$ and signal acquisition. For both crystals, a spin-exchange mixing time of 10 sec was used. Spectra from MMHH experiments (Fig. 2F) were acquired at 55 kHz with SPINAL-16 ^{1}H decoupling at 55 kHz, and SPINAL-16 ^{2}H decoupling at 20 kHz during t$_1$ and t$_2$ intervalsin. In these experiments, 32 scans were acquired, for 64 t$_1$ points with 100 μsec dwell times in the indirect dimension. The experiments utilized 4 sec z-filter and 10 msec mismatched Hartmann-Hahn irradiations. The levels of Hartmann-Hahn mismatch during the spin lock were 15% for the protiated NAL crystal and 5% for the perdeuterated NAL crystal.

Data processing was performed using the software programs NMRPipe [32] and Topspin 3.1 (www.bruker.com).

3. Results

3.1. ^{2}H decoupling

The spectra in Fig. 3 demonstrate the broadening effect of nearby deuterons on ^{15}N resonances. In the NAL crystal, the ^{1}H nuclei on carbon sites contribute 200–250 Hz to the ^{15}N resonance line-widths (Fig. 3C). The effects of perdeuteration on the spectra are different for in Pf1 coat protein, where the broadening is reduced by the rapid rotational diffusion of the membrane-bound form of the protein in the bilayer environment (Fig. 3F). Application of ^{2}H decoupling attenuates the broadening effects of the deuterons on the ^{15}N sites, resulting in narrow lines in the perdeuterated samples (Fig. 3(B and E)). In Fig. 3A the frequencies of the 4 resonances differ compared to those in Fig. 3(B and C) due to slight differences in the crystal orientation. The frequencies of the deuterium sites are measured with the quadruple-echo experiment (Fig. 4;B) the furthest resonance from the center of the spectrum resides at ±59 kHz. The orientation of the crystal used to obtain the data in Fig. 4A is slightly different from that used in Fig. 3A and C. The large quadrupole splittings shown in Fig. 4B illustrate the challenges in decoupling ^{2}H from ^{15}N if the conventional single quantum decoupling process is considered.

The power requirements for ^{2}H decoupling were determined using the data shown in Fig. 5. The ^{1}H decoupling power is fixed and the power of the irradiation at the ^{2}H resonance frequency is varied between 0 kHz and 30 kHz for the single crystal sample (Fig. 5A), and between 0 kHz and 20 kHz for the aligned membrane protein sample (Fig. 5B). Complete ^{2}H decoupling of the stationary NAL single crystal sample requires 20 kHz of power while the oriented Pf1 coat protein sample undergoing rotational diffusion requires only 10 kHz of power. Significantly, perdeuterated NAL with adequate ^{1}H and ^{2}H decoupling (Fig. 3B) and protiated NAL with ^{1}H decoupling (Fig. 3A) have similar ^{15}N resonance line-widths. Perdeuteration also did not affect the ^{15}N resonance line-widths of a ^{1}H back-exchanged sample of uniformly ^{2}H and ^{15}N labeled Pf1 coat protein in bicelles (Fig. 3E) compared to those of the protiated sample (Fig. 3D).

The fully decoupled spectra of NAL and of membrane-bound Pf1 coat protein have 15N resonance line-widths of ~140 Hz and ~90 Hz, respectively. The representation of the unit cell for the perdeuterated NAL single crystal shown in Fig. 4D is based on the crystal structure (CCDC 624793 [34]). At the crystal orientation that gives the ^{15}N NMR spectrum shown Fig. 4A the corresponding ^{2}H NMR spectrum was obtained with the quadrupole-echo experiment (Fig. 4B). For comparison, a simulated rigid lattice ^{2}H NMR powder pattern for a typical C-D bond is shown with the solid line and the corresponding spectrum for a CD_3 group undergoing rapid three-fold reorientation is shown with the dashed line in Fig. 4C.

3.2. ^{1}H decoupling

The one-dimensional ^{15}N NMR spectra in Fig. 6 were acquired with adequate ^{2}H decoupling and variable levels of ^{1}H decoupling. The goal was to determine whether deuteration of the carbon sites affects the radiofrequency power required to decouple the ^{1}H from the ^{15}N at the labeled amide sites in the NAL crystal and in the oriented membrane protein sample. Narrow ^{15}N resonance line-widths were obtained only when the ^{1}H power

was greater than 30 kHz; notably, the power required for complete ^{1}H decoupling did not differ between NAL samples with ^{1}H or ^{2}H bonded to the carbon sites. Similarly, the protein samples required ^{1}H power greater than 20 kHz for decoupling, regardless of whether the carbon sites were deuterated or not. The data in Fig. 6 show that perdeuteration does not reduce the magnitude of the ^{1}H irradiation required to effect heteronuclear decoupling in stationary samples of crystals or oriented proteins in hydrated phospholipid bilayers.

3.3. ^{1}H-^{15}N dipolar coupling

Perdeuteration has a significant effect on line-widths in the heteronuclear dipolar coupling frequency dimension of separated local field (SLF) spectra (Fig. 7(B and D)). The resonance line-widths of the perdeuterated samples are significantly narrower in Fig. 7(B and D) than those in Fig. 7(A and C). The narrowest line-width observed from the protiated NAL crystal is 2.2 kHz (marked with an arrow in Fig. 7A), in contrast the narrowest line-width is 0.85 kHz for the perdeuterated sample (marked with an arrow in Fig. 7B). Similar levels of line-width reduction are observed in samples of the membrane protein with perdeuteration (Fig. 7(C and D)). In CP buildup curves, the perdeuterated samples have their dipolar oscillations extend longer than 1 msec (Fig. 8(B and D)), which is consistent with the deuterons isolating the ^{1}Hnuclei. Notably, improvements in the line-widths of the heteronuclear dipolar couplings in the perdeuterated samples were not observed in SAMPI4 experiments (Fig. 9).

3.4. ^{1}H-^{15}N HETCOR

The results of two-dimensional ^{1}H-^{15}N heteronuclear correlation (HETCOR) experiments, where the ^{1}H chemical shift evolves under FSLG magic angle ^{1}H-^{1}H homonuclear decoupling during the t_1 interval are shown in Fig. 10. The arrows point to the signals selected for analysis in the ^{1}H chemical shift frequency dimension; the corresponding spectral slices are plotted along the vertical-axis. The vertical-axis is the ^{1}H chemical shift dimension obtained in the presence of both ^{1}H-^{1}H homonuclear and ^{1}H-^{15}N heteronuclear decoupling applied during the t_1 interval. The ^{1}H line-width observed in the perdeuterated NAL crystal spectrum (560 Hz, Fig. 10B) and that from the protiated crystal (670 Hz, Fig. 10A) are similar. Comparable results were obtained for the oriented Pf1 coat protein under the same conditions (Fig. 10(C and D)).

3.5. Spin-exchange experiments

PDSD spin-exchange experiments were performed on both protiated (Fig. 11(A–C)) and perdeuterated (Fig. 11(D–F)) NAL crystals. Similar cross-peak intensities were observed for both samples (Fig. 11(C vs. F)). Because the two crystals have slightly different orientations in the magnetic field, cross-peak intensities are more clearly compared in the slices (Fig. 11(B and E)) rather than the contour plots (Fig. 11(C and F)). In the MMHH experiment (Fig. 12), however, stronger diagonal and cross-peak intensities are observed in the spectra of the perdeuterated NAL crystal (Fig. 12(E and F)) than of the protiated NAL crystal (Fig. 12(B and C)). To facilitate the presentation of the results in Fig. 12, the spectra are further analyzed in Fig. 13. First of all, horizontal slices through each diagonal resonances are shown in Fig. 13(A and B). The diagonal resonances are distinguished from the off-diagonal resonances by asterisks. It can be easily seen from the one-dimensional slices that all off-diagonal resonances are present; this is in contrast to the two-dimensional spectra shown in

Fig. 12 where one of the weakest off-diagonal resonances in each spectrum cannot be seen because it is too close to the noise levels. To demonstrate the levels of sensitivity enhancement in the MMHH experiment due to perdeuteration, the intensities of the resonances in the two-dimensional spectra shown in Fig. 12 are quantified, normalized, and ranked in Fig. 13C. Because the two crystals are not at the same orientation, comparisons cannot be made by examining the resonances with the same chemical shifts. To demonstrate the variable intensities of the resonances in the two-dimensional spectra, we chose the method of ranking the resonances based on their measured intensities. Comparisons of the intensity distribution ranked from high-to-low for the two crystals demonstrate that with perdeuteration, significant sensitivity enhancements can be obtained for the diagonal resonances, while lower levels of enhancements can be obtained with the off-diagonal resonances. The intensities shown in Fig. 13C are raw S/ N values measured from data in Fig. 13(A and B), and not subject to adjustments based on the crystal sizes.

4. Discussion

Deuteration affects the signals from nearby sites, although there is minimal chemical perturbation from the additional neutron in deuterons compared to protons. The specific goal of these experimental studies is to explore the use of deuteration to improve the resolution and sensitivity of multidimensional solid-state NMR experiments on stationary samples, such as single crystals and uniaxially aligned proteins. To understand the effects of deuteration, comparisons were made between similarly prepared protiated and perdeuterated samples. In the spectra of the protiated NAL single crystal, acquired with ^{1}H decoupling, ~140 Hz ^{15}N resonance line-widths were observed. In the spectra of the perdeuterated NAL single crystal, ~140 Hz ^{15}N resonance line-widths were only observed when both ^{1}H and ^{2}H decoupling was applied. Because ^{2}H has a different NMR frequency than ^{1}H, their presence on proximate carbon sites requires a separate RF channel for decoupling. This is why two ^{1}H, ^{2}H, ^{15}N triple-resonance NMR probes were built for the experiments of the perdeuterated NMR samples.

Irradiation at the ^{2}H resonance frequency causes rapid transitions between the ^{2}H nuclear spin states. When the irradiation power is strong enough, spins are decoupled from one another. Due to the large ^{2}H quadrupole splittings, very high-power irradiation would be required for single-quantum decoupling. Importantly, it has been shown that spin $S = 1$ ^{2}H nuclei at magnetic field strengths less than the amplitudes of the quadrupole couplings can be decoupled through a double quantum process [8,35].

When the ^{2}H quadrupole splitting for the C_a deuterons is on the order of 180 kHz and the ^{2}H-^{15}N dipolar splitting is on the order of 250 Hz, the decoupling field strength required for double quantum decoupling is only on the order of $(QD)^{\frac{1}{2}}$ compared to Q for single quantum decoupling [8], where Q is the quadrupole coupling constant and D is the dipolar coupling constant. Given the orders of magnitude differences between Q and D, the required field strength is then lowered from hundreds of kHz to tens of kHz. This is in agreement with experimental findings when SPINAL-16 is used to minimize the effects of frequency offsets due to chemical shielding where the decoupling power required is less than 50 kHz for the rigid crystal sample and much less for motional averaged protein samples.

Signals from different crystals of the same compound can have different line-widths due to a variety of factors such as crystal packing. Small differences in line-widths could be attributed to such effects. [36] In addition, anisotropic chemical shifts depend on the crystal orientation, which can be adjusted by rotating the crystal within the sample coil. This is why the frequencies of the resonances are different in many of the spectra of the single crystal samples. Magnetically oriented Pf1 coat proteins in lipid bilayers, by comparison, self-orient to the same orientation [37]. Thus, comparisons among different protein samples are simpler, because their spectra have matching resonance frequencies.

Whether the ^{15}N resonance line-widths or the power requirements for decoupling the protiated and perdeuterated samples are compared, the results are similar. This is the case for both the NAL single crystal sample and the magnetically aligned Pf1 coat protein sample. This result suggests that carbon site perdeuteration alone is not sufficient to further reduce ^{15}N line-widths in peptide samples. Effects of ^{1}H dilution were observed in SLF experiments for both the perdeuterated NAL crystal and the perdeuterated oriented membrane protein sample. The dipolar coupling frequency line-widths in both samples are much reduced in the absence of ^{1}H-^{1}H homonuclear decoupling during t_1. Based on the differences in line-widths between the protiated (2.2 kHz) and perdeuterated NAL crystals (0.85 kHz), SLF experiments show that the contribution of line-widths from the ^{1}H on nearby carbon sites is approximately 1.35 kHz. Here perdeuteration can be applied where the use of high-power irradiation is limited by instrumentation or sample heating. In contrast, in experiments where the ^{1}H-^{1}H homonuclear dipolar couplings are attenuated, such as with SAMPI4, line-narrowing was not observed in the perdeuterated samples. The absence of further line-narrowing by homonuclear decoupling on the perdeuterated samples suggests that the homonuclear decoupling and perdeuteration operate on the same line broadening mechanisms and their effects are not additive.

Resonances in the HETCOR spectra shown in Fig. 10(A and B) are tilted in appearance for the NAL single crystal samples, this was previously observed by Lu et al. (2012). The explanation for the observation of the tilted resonances, however, is beyond the scope of this paper.

Remarkably, the results of passive homonuclear spin-exchange experiments are not altered by the presence of high levels of deuteration on single crystal samples. This suggests that the mechanism of homonuclear spin-exchange does not require the presence of strong and ^{1}H-^{1}H dipolar couplings. In each protiated NAL molecule there are thirteen ^{1}H bonded to carbons, one bonded to nitrogen and one bonded to oxygen; in the "perdeuterated" case, there are no ^{1}H bonded to carbon, one bonded to nitrogen, and one bonded to oxygen. Thus, in the crystalline samples, the presence of ^{1}H is reduced from 100% to 13% by synthesis of the perdeuterated samples. If the dominant mechanism of spin-exchange is through the "abundant" ^{1}H spin bath, then different spin-exchange dynamics would be expected in highly deuterated samples. We have no evidence that this is the case. One explanation for the lack of difference might be that dilute spin-exchange is playing a role here. The possibility of the dominant role of dilute spin-exchange mechanism was demonstrated previously in unenriched organic solids [38]. In contrast, a proton relay mechanism, such as that proposed for the MMHH experiment only requires two nearby ^{1}H for each ^{15}N spin pair and is not

directly affected by "perdeuteration" of many carbon sites. Dilute spin-exchange works well on samples of perdeuterated NAL with as little as 5% Hartmann-Hahn mismatch. By contrast, protiated NAL requires at least 10–15% Hartmann-Hahn mis-match to give measurable on- and off-diagonal resonances. This is because in the perdeuterated NAL crystal, there are fewer ^{1}H available to drain the ^{15}N magnetization during the MMHH mixing period. As a result, the experiments yield stronger signals. In addition, because MMHH works well at lower levels of Hartmann-Hahn mis-match on the perdeuterated NAL single crystal, the mixing is more efficient which results in stronger off-diagonal signals. In this case, even though the perdeuterated crystal is significantly smaller in size, acquisition of the same number of scans results in stronger or equal intensity on and off-diagonal signals.

5. Conclusions

Perdeuteration isolates ^{1}H nuclei in organic and biochemical molecules. It reduces most of the effects of the ^{1}H-^{1}H spin network on individual resonances and it prolongs the ^{1}H-^{15}N heteronuclear dipolar coupling evolution in SLF experiments. However, perdeuteration is not as effective as ^{1}H-^{1}H homonuclear decoupling in oriented sample solid-state NMR. This is because the ^{1}H back-exchange step leaves proximate ^{1}H nuclei, which still require substantial ^{1}H-^{1}H homonuclear decoupling. In, sensitivity enhancement due to deuteration was observed in the spin-diffusion experiments that utilized the mis-match Hartmann-Hahn mechanism.

Acknowledgements

References

[1]. Crespi HL, Rosenber RM, Katz JJ, Proton magnetic resonance of proteins fully deuterated except for 1h-leucine side chains, Science 161 (1968) 796–1000. [PubMed: 5663809]

[2]. Markley JL, Putter I, Jardetzky O, High-resolution nuclear magnetic resonance spectra of selectively deuterated staphylococcal nuclease, Science 161 (1968), 1249–+. [PubMed: 5673435]

[3]. Mcdermott AE, Creuzet FJ, Kolbert AC, Griffin RG, High-resolution magic-angle-spinning NMR-spectra of protons in deuterated solids, J. Magn. Reson 98 (1992) 408–413.

[4]. Morcombe CR, Paulson EK, Gaponenko V, Byrd RA, Zilm KW, H-1-N-15 correlation spectroscopy of nanocrystalline proteins, J. Biomol. NMR 31 (2005) 217–230. [PubMed: 15803395]

[5]. Reif B, Jaroniec CP, Rienstra CM, Hohwy M, Griffin RG, H-1-H-1 MAS correlation spectroscopy and distance measurements in a deuterated peptide, J. Magn. Reson 151 (2001) 320–327. [PubMed: 11531354]

[6]. Hewitt RC, Meiboom S, Snyder LC, Proton NMR in nematic liquid crystalline solvents – use of deuterium decoupling, J. Chem. Phys 58 (1973) 5089–5095.

[7]. Snyder LC, Meiboom S, Theory of proton NMR with deuteron decoupling in nematic liquid crystalline solvents, J. Chem. Phys 58 (1973) 5096–5103.

[8]. Pines A, Ruben DJ, Vega S, Mehring M, New approach to high-resolution proton NMR in solids – deuterium spin decoupling by multiple-quantum transitions, Phys. Rev. Lett 36 (1976) 110–113.

[9]. Goldburg WI, Lee M, Nuclear magnetic resonance line narrowing by a rotating rf field, Phys. Rev. Lett 11 (1963) 255–258.

[10]. Bielecki A, Kolbert AC, De Groot HJM, Griffin RG, Levitt MH, Frequency-switched Lee—Goldburg sequences in solids, in: Warren WS (Ed.), Advances in Magnetic and Optical Resonance, Academic Press, 1990, pp. 111–124.

[11]. Waugh JS, Huber LM, Haeberlen U, Approach to high-resolution NMR in solids, Phys. Rev. Lett 20 (1968), 180–+.

[12]. Pines A, Rhim W, Waugh JS, Homogeneous and inhomogeneous nuclear spin echoes in solids, J. Magn. Reson 6 (1972) 457–1000.

[13]. Hester RK, Ackerman JL, Neff BL, Waugh JS, Separated local field spectra in NMR – determination of structure of solids, Phys. Rev. Lett 36 (1976) 1081–1083.

[14]. Waugh JS, Uncoupling of local field spectra in nuclear magnetic-resonance – determination of atomic positions in solids, Proc. Natl. Acad. Sci. USA 73 (1976) 1394–1397. [PubMed: 1064013]

[15]. Wu CH, Ramamoorthy A, Opella SJ, High-resolution heteronuclear dipolar solid-state NMR-spectroscopy, J. Magn. Reson. Ser. A 109 (1994) 270–272.

[16]. Nevzorov AA, Opella SJ, A "Magic Sandwich" pulse sequence with reduced offset dependence for high-resolution separated local field spectroscopy, J. Magn. Reson 164 (2003) 182–186. [PubMed: 12932472]

[17]. Nevzorov AA, Opella SJ, Selective averaging for high-resolution solid-state NMR spectroscopy of aligned samples, J. Magn. Reson 185 (2007) 59–70. [PubMed: 17074522]

[18]. Park SH, Marassi FM, Black D, Opella SJ, Structure and dynamics of the membrane-bound form of Pf1 coat protein: implications of structural rearrangement for virus assembly, Biophys. J 99 (2010) 1465–1474. [PubMed: 20816058]

[19]. Park SH, Opella SJ, Triton X-100 as the "Short-Chain Lipid" improves the magnetic alignment and stability of membrane proteins in phosphatidylcholine bilayers for oriented-sample solid-state NMR spectroscopy, J. Am. Chem. Soc 132 (2010) 12552–12553. [PubMed: 20735058]

[20]. Bloembergen N, On the interaction of nuclear spins in a crystalline lattice, Physica 15 (1949) 386–426.

[21]. Suter D, Ernst RR, Spin diffusion in resolved solid-state NMR-spectra, Phys. Rev. B 32 (1985) 5608–5627.

[22]. Szeverenyi NM, Sullivan MJ, Maciel GE, Observation of spin exchange by two-dimensional fourier-transform C-13 cross polarization-magic-angle spinning, J. Magn. Reson 47 (1982) 462–475.

[23]. Nevzorov AA, Mismatched Hartmann-Hahn conditions cause proton-mediated intermolecular magnetization transfer between dilute low-spin nuclei in NMR of static solids, J. Am. Chem. Soc 130 (2008) 11282–11283. [PubMed: 18680251]

[24]. Lu GJ, Opella SJ, Mechanism of dilute-spin-exchange in solid-state NMR, J. Chem. Phys 140 (2014).

[25]. Carroll PJ, Stewart PL, Opella SJ, Structures of two model peptides: N-acetyld, l-valine and N-acetyl-l-valyl-l-leucine, Acta Crystallogr. Sect. C 46 (1990) 243–246.

[26]. Thiriot DS, Nevzorov AA, Zagyanskiy L, Wu CH, Opella SJ, Structure of the coat protein in Pf1 bacteriophage determined by solid-state NMR spectroscopy, J. Mol. Biol 341 (2004) 869–879. [PubMed: 15288792]

[27]. Park SH, Yang C, Opella SJ, Mueller LJ, Resolution and measurement of heteronuclear dipolar couplings of a noncrystalline protein immobilized in a biological supramolecular assembly by proton-detected MAS solid-state NMR spectroscopy, J. Magn. Reson 237 (2013) 164–168. [PubMed: 24225529]

[28]. Schiksnis RA, Bogusky MJ, Tsang P, Opella SJ, Structure and dynamics of the Pf1 filamentous bacteriophage coat protein in micelles, Biochemistry 26 (1987) 1373–1381. [PubMed: 3567175]

[29]. McNeill SA, Gor'kov PL, Shetty K, Brey WW, Long JR, A low-E magic angle spinning probe for biological solid state NMR at 750 MHz, J. Magn. Reson 197 (2009) 135–144. [PubMed: 19138870]

[30]. Sinha N, Grant CV, Wu CH, De Angelis AA, Howell SC, Opella SJ, SPINAL modulated decoupling in high field double- and triple-resonance solid-state NMR experiments on stationary samples, J. Magn. Reson 177 (2005) 197–202. [PubMed: 16137902]

[31]. Lu GJ, Park SH, Opella SJ, Improved 1H amide resonance line narrowing in oriented sample solid-state NMR of membrane proteins in phospholipid bilayers, J. Magn. Reson 220 (2012) 54–61. [PubMed: 22683581]

[32]. Delaglio F, Grzesiek S, Vuister GW, Zhu G, Pfeifer J, Bax A, NMRPipe: a multidimensional spectral processing system based on UNIX pipes, J. Biomol. NMR 6 (1995) 277–293. [PubMed: 8520220]

[33]. Colnago LA, Valentine KG, Opella SJ, Dynamics of Fd-coat protein in the bacteriophage, Biochemistry-Us 26 (1987) 847–854.

[34]. Rheingold AL, CCDC 624793: Experimental Crystal Structure Determination, 2014.

[35]. Pines A, Vega S, Mehring M, NMR double-quantum spin decoupling in solids, Phys. Rev. B 18 (1978) 112–125.

[36]. Prigl RH, U., The Theoretical and Practical Limits of Resolution in Multiple-Pulse High-Resolution NMR of Solids, Academic Press, San Diego, 1990.

[37]. Park SH, Mrse AA, Nevzorov AA, De Angelis AA, Opella SJ, Rotational diffusion of membrane proteins in aligned phospholipid bilayers by solid-state NMR spectroscopy, J. Magn. Reson 178 (2006) 162–165. [PubMed: 16213759]

[38]. Virlet J, Ghesquieres D, NMR longitudinal cross relaxation induced by natural abundance ^{13}C–^{13}C dipolar interaction in organic solids. Hexamethylethane, Chem. Phys. Lett 73 (1980) 323–327.
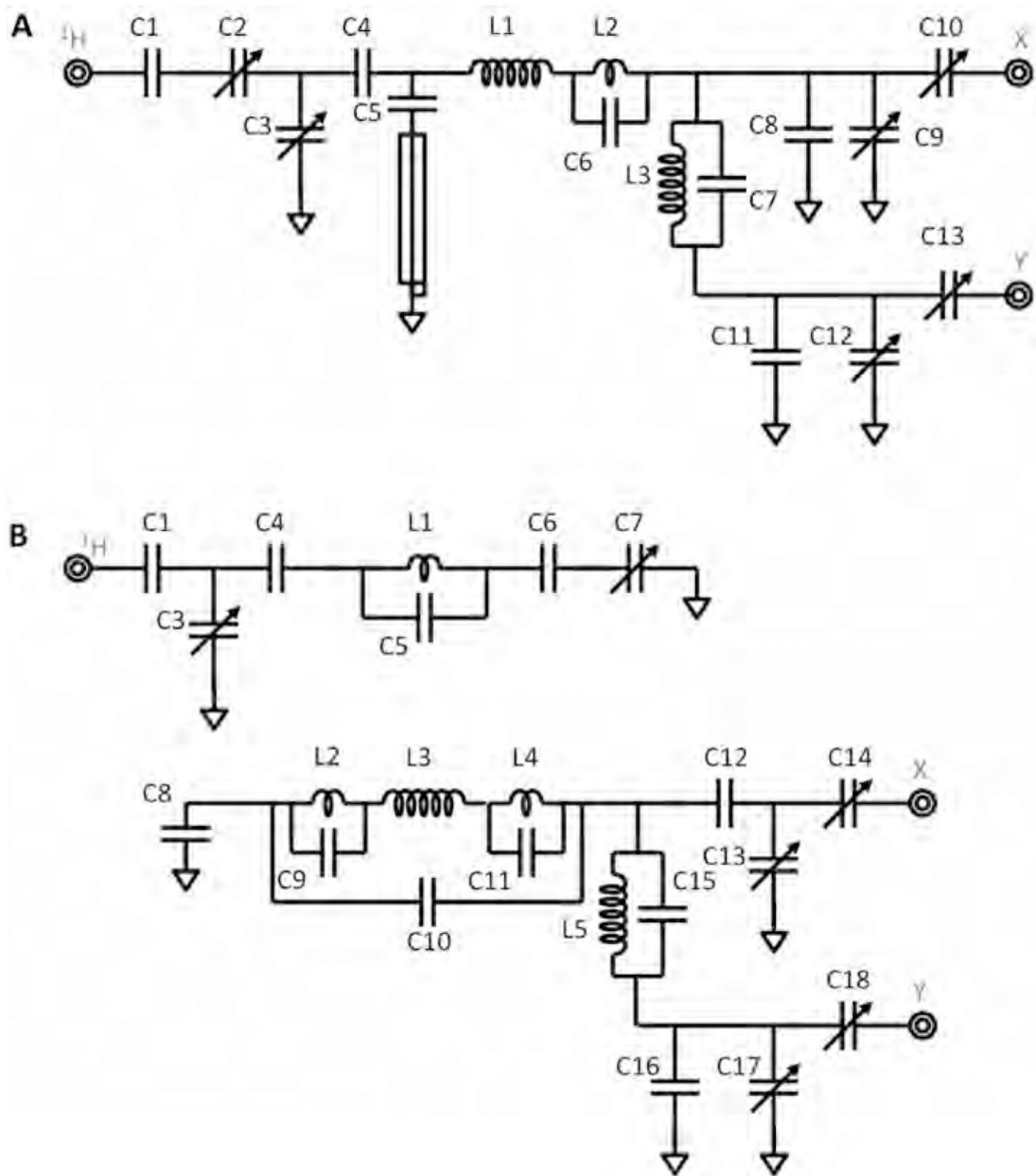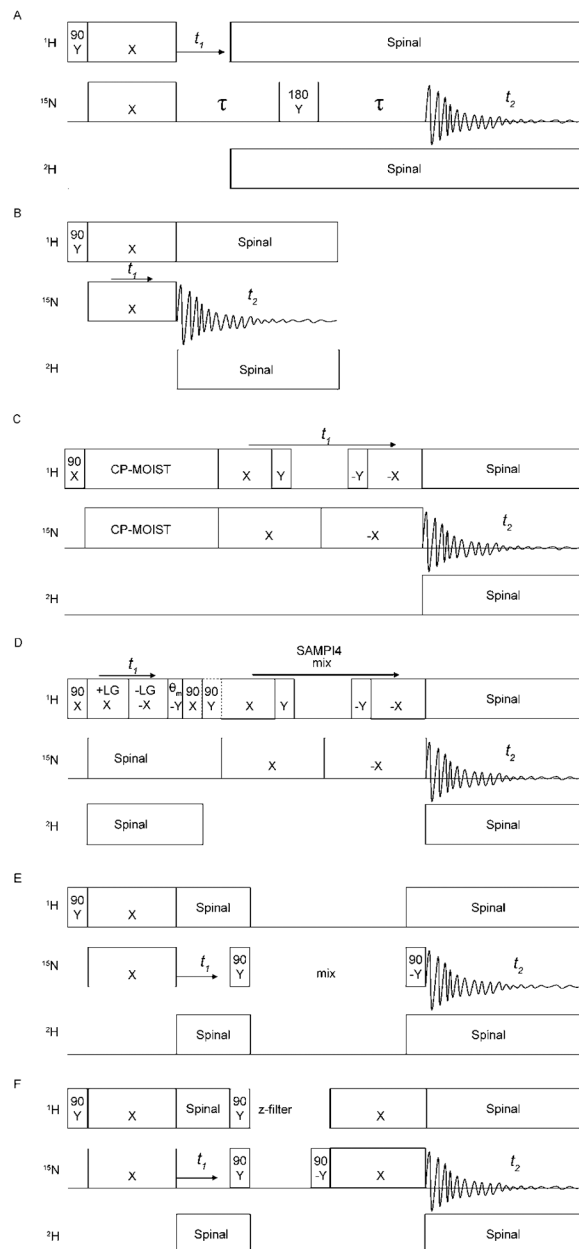
Fig. 1.
Circuit diagrams for triple-resonance HDN probes using (A) a single solenoid coil (L1) and (B) a cross-coil assembly with a loop-gap resonator (L1) and a solenoid coil (L3).

Fig. 2.
Timing diagrams of pulse sequences utilized to obtain the experimental data presented in the figures. (A) Two-dimensional separated local field (SLF) experiment with no decoupling during t_1 and both ^1H and ^2H decoupling applied during data acquisition t_2. The 180° pulse refocuses the ^{15}N chemical shift. (B) One-dimensional cross-polarization (CP) experiment where the interval for magnetization transfer is varied. ^1H and ^2H decoupling are applied during data acquisition. The intensities of individual signals are monitored as a function of time, as illustrated in Fig. 8. (C) SAMPI4 experiment with ^1H and ^2H decoupling applied during data acquisition t_2. (D) Heteronuclear correlation (HETCOR) experiment with ^1H and ^2H decoupling applied during the incremented t_1 period and data acquisition t_2. (E) Proton-driven spin diffusion (PDSD) experiment with ^1H and ^2H decoupling applied during

the incremented t_1 period and data acquisition t_2. (F) Mismatched Hartmann-Hahn (MMHH) experiment with ^{1}H and ^{2}H decoupling applied during the incremented t_1 period and data acquisition t_2.
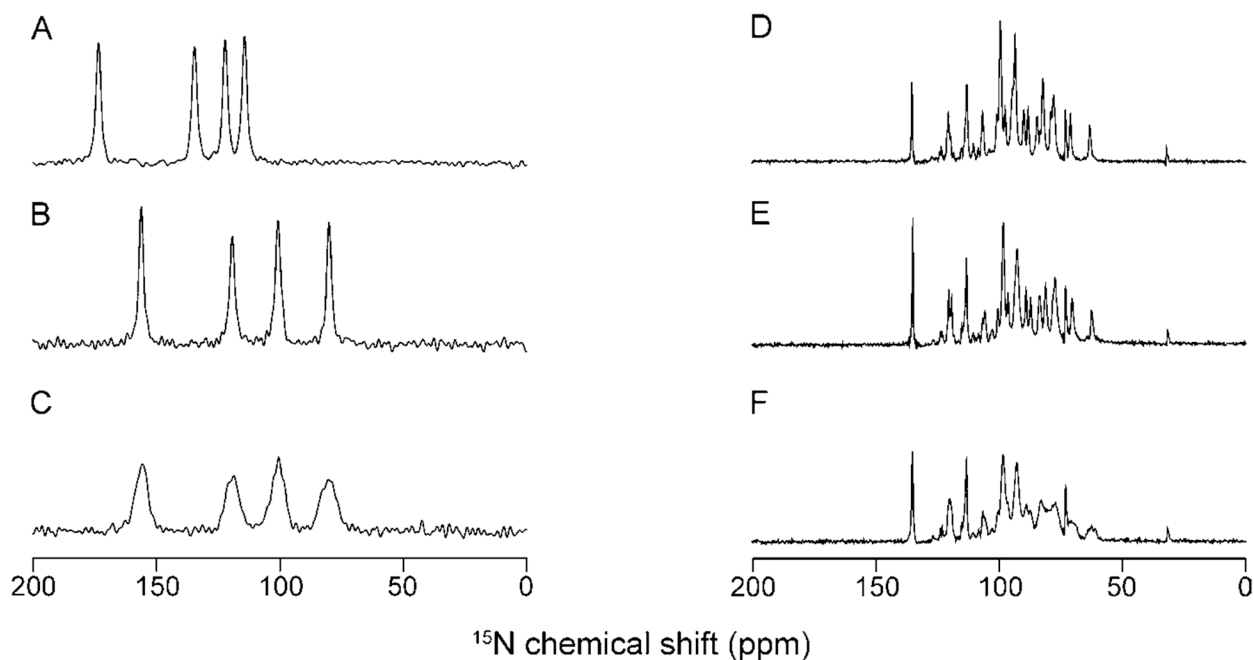
Fig. 3.

Experimental ^{15}N NMR spectra showing the effects of ^{2}H decoupling on ^{1}H decoupled ^{15}N resonances. The ^{1}H resonance frequency was 700 MHz for spectra (A–C) and 900 MHz for spectra (D–F). (A) Protiated ^{15}N labeled NAL single crystal. (B and C) Perdeuterated ^{15}N labeled NAL single crystal. (D) Uniformly ^{15}N labeled Pf1 coat protein. (E and F) Perdeuterated and uniformly ^{15}N labeled Pf1 coat protein. The protein samples in (D–F) were oriented in DMPC: Triton X-100 $q = 5$ bicelles with their bilayer normals perpendicular to the direction of the magnetic field. Spectra (B) and (E) were acquired with the application of 20 kHz and 10 kHz SPINAL-16 ^{2}H decoupling, respectively. Spectra (C and F) were acquired without ^{2}H decoupling during data acquisition. Spectra (A–C) were acquired with the application of 50 kHz SPINAL-16 ^{1}H decoupling during the 10 msec acquisition time. Spectra (D–F) were acquired with the application of 45 kHz SPINAL-16 ^{1}H decoupling during the 20 msec acquisition time.
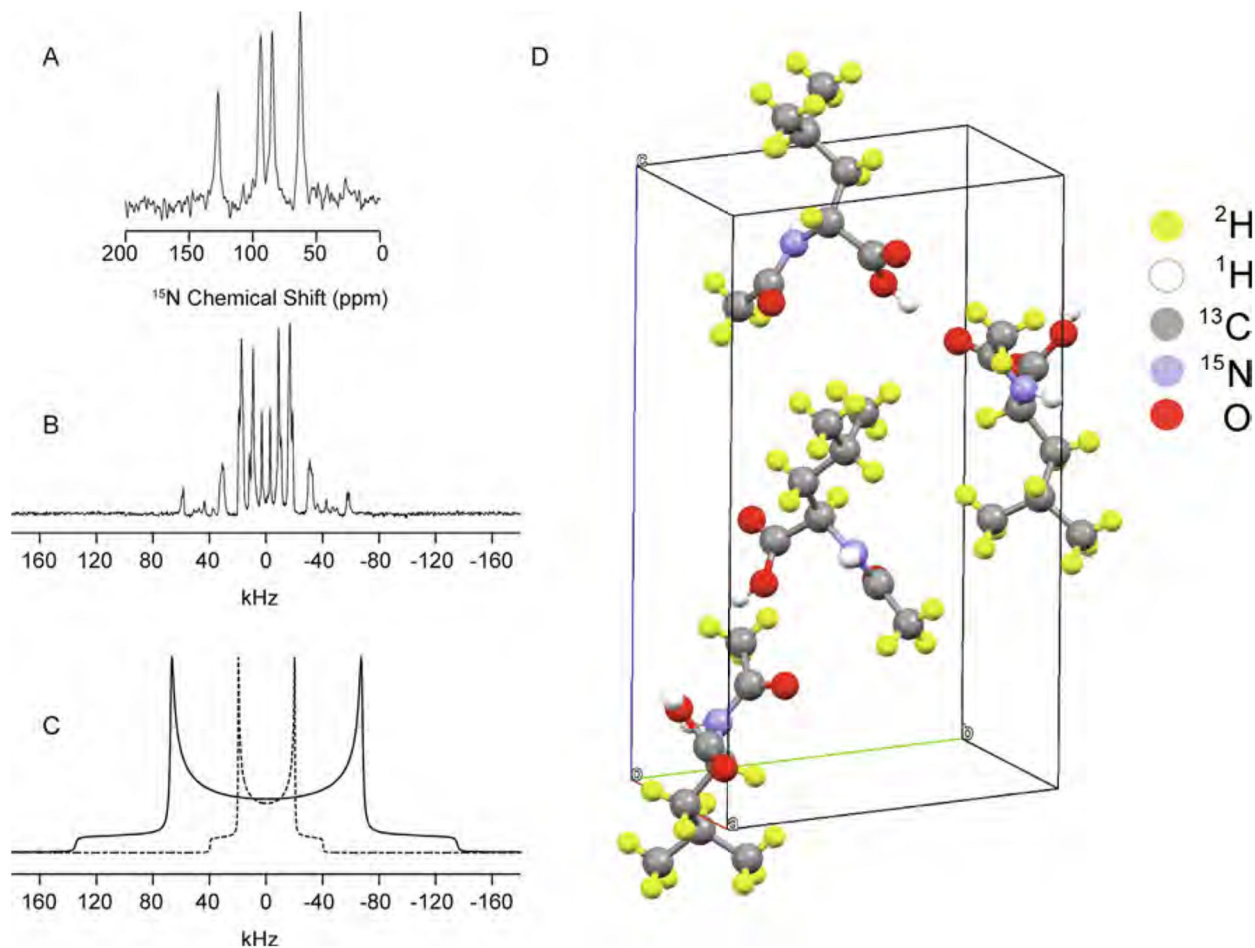
Fig. 4.
(A) ^{15}N NMR spectrum of the perdeuterated ^{15}N labeled NAL crystal used in Fig. 3 with 50 kHz ^{1}H SPINAL-16 and 40 kHz ^{2}H SPINAL-16 decoupling applied during data acquisition. (B) ^{2}H NMR spectrum obtained with [2]H 55 kHz pulses during the quadrupole-echo experiment at the same crystal orientation as (A). 55 kHz ^{1}H SPINAL-16 decoupling was applied during signal acquisition. (C) Calculated powder patterns for the CD (solid line) and CD_3 sites (dashed line) on perdeuterated NAL [33]. (D) An illustration of the unit cell of the NAL single crystal. The ^{2}H atoms shown in yellow are placed in the positions predicted for the ^{1}H atoms based on the NAL crystal structure [34].
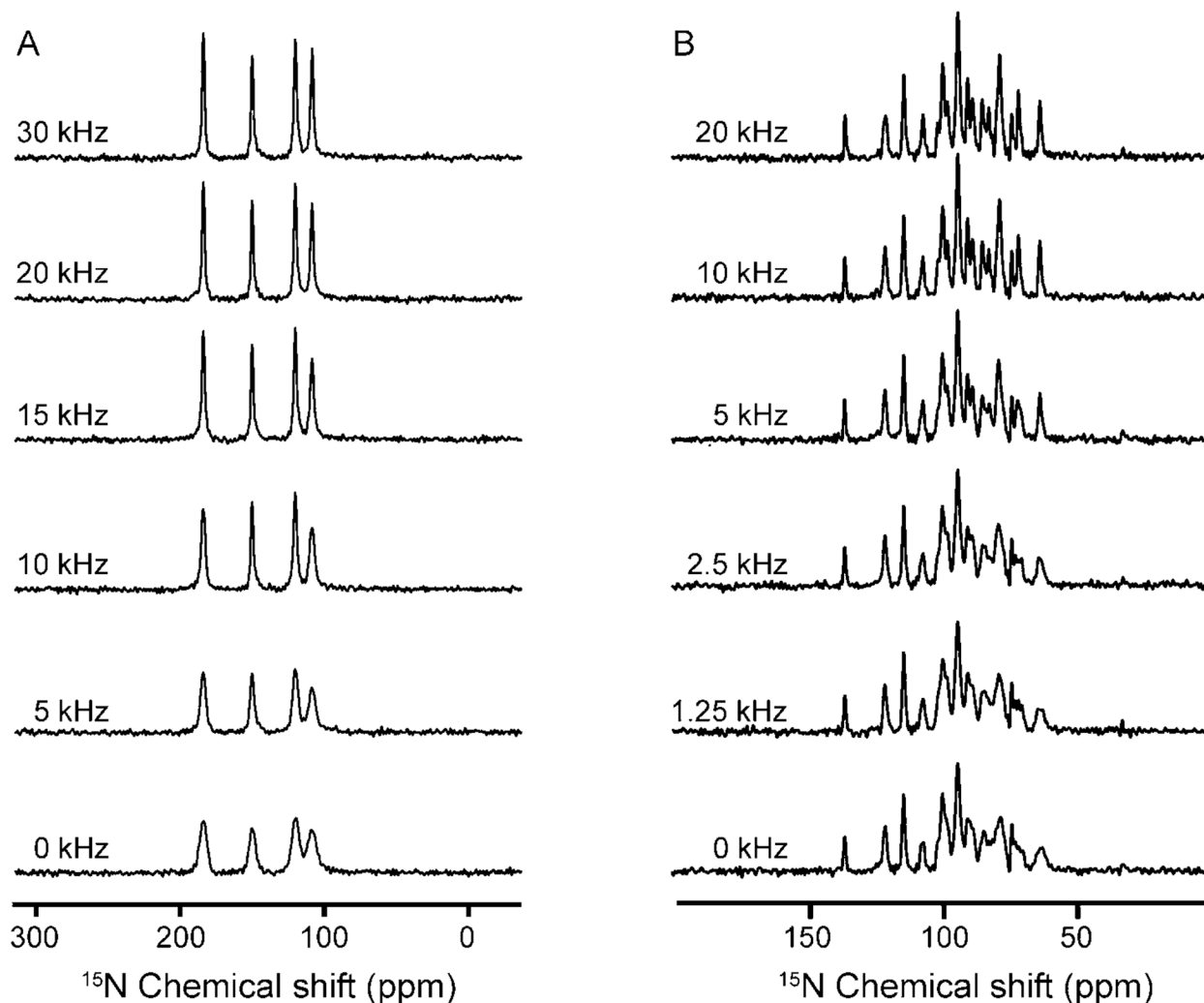
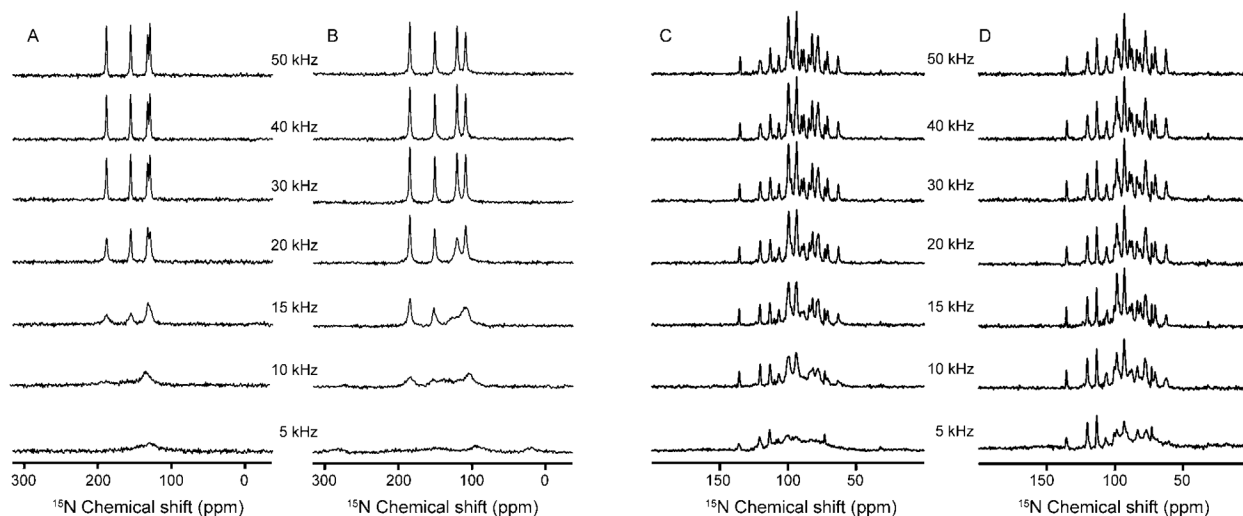**Fig. 5.**
Effects of ^{2}H decoupling on ^{1}H decoupled ^{15}N resonances. The ^{1}H resonance frequency was 700 MHz for (A) and 900 MHz for (B). (A) Perdeuterated ^{15}N labeled NAL single crystal. (B) Uniformly ^{15}N and ^{2}H labeled Pf1 coat protein (^{1}H back-exchanged) in DMPC: Triton X-100 $q = 5$ bicelles oriented with their bilayer normals perpendicular to the direction of the magnetic field. Spectra in (A) and (B) were acquired with 50 kHz ^{1}H SPINAL-16 decoupling. As marked in the figures, the spectra were acquired with SPINAL-16 modulated ^{2}H irradiation during data acquisition with radiofrequency powers ranging from 0 kHz to 30 kHz (A), and 0 kHz to 20 kHz (B).

Fig. 6.
Effects of ^{1}H decoupling on ^{2}H decoupled ^{15}N resonances. The ^{1}H resonance frequency was 700 MHz for the spectra in (A) and (B) and 900 MHz for the spectra in (C) and (D). (A) Protiated ^{15}N labeled NAL single crystal at an arbitrary orientation. (B) Perdeuterated ^{15}N labeled NAL single crystal at a similar orientation. (C) Uniformly ^{15}N labeled Pf1 coat protein in DMPC: Triton X-100 $q = 5$ bicelles. (D) Uniformly ^{2}H and ^{15}N labeled Pf1 coat protein (^{1}H back-exchanged) in DMPC: Triton X-100 $q = 5$ bicelles. (C) and (D) were oriented with the bilayer normals perpendicular to the direction of the magnetic field. All spectra in (B) were acquired with 20 kHz ^{2}H SPINAL-16 decoupling, and all spectra in (D) were acquired with 10 kHz ^{2}H SPINAL-16 decoupling. As marked in the figure, the spectra were acquired with ^{1}H SPINAL-16 irradiation at radiofrequency powers ranging between 5 kHz and 50 kHz.
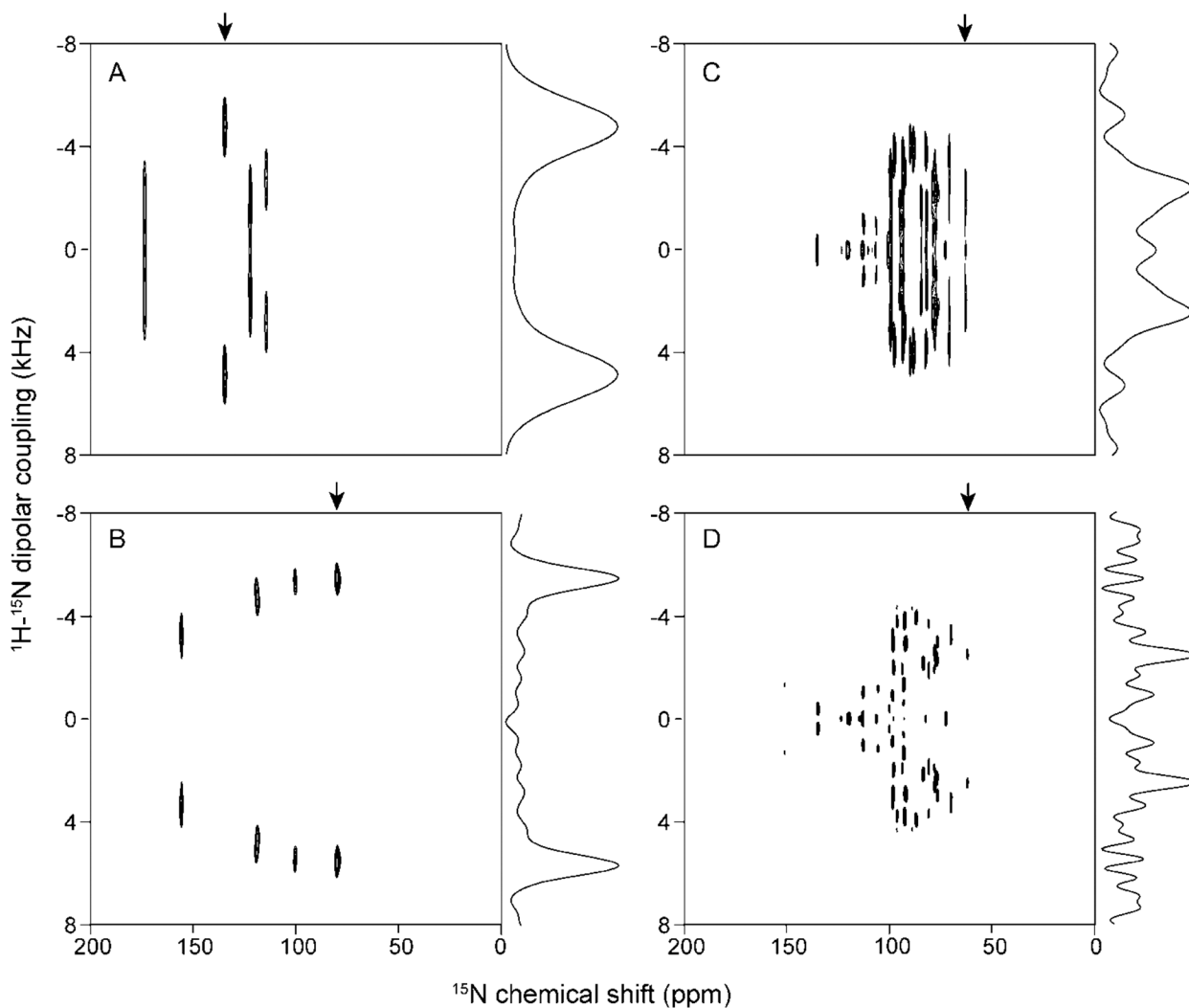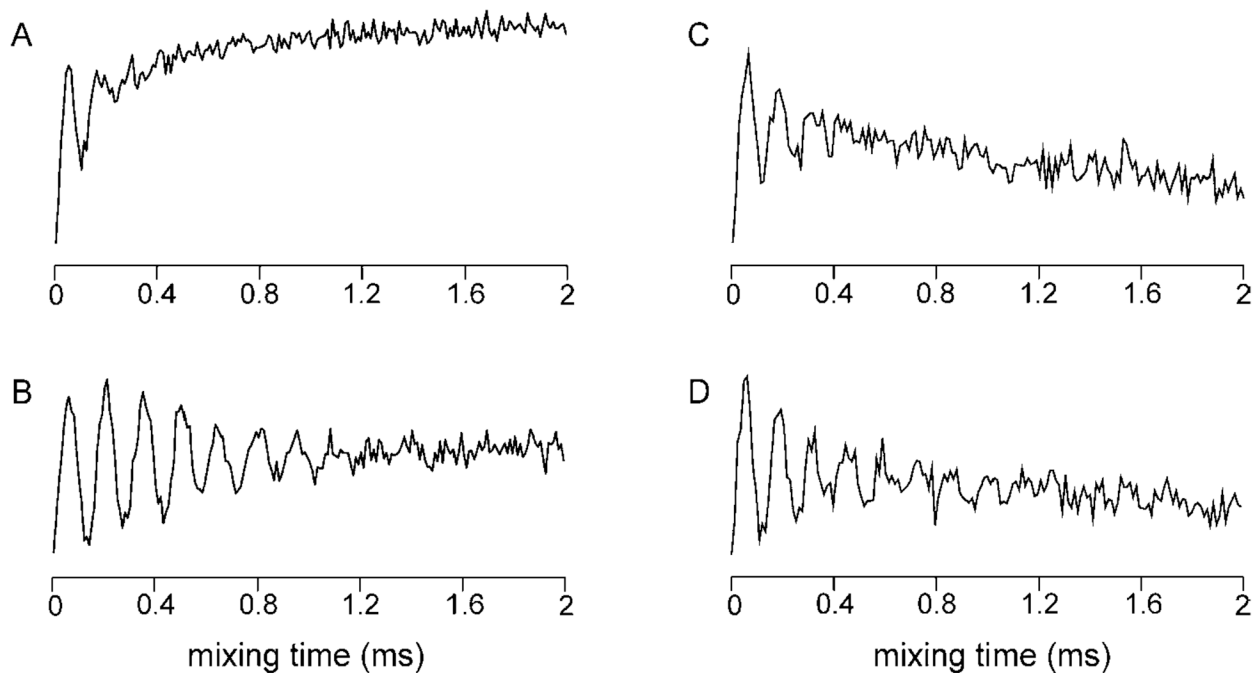
Fig. 7.
Effects of perdeuteration on two-dimensional ^{1}H-^{15}N SLF spectra. The ^{1}H resonance frequency was 700 MHz for spectra (A) and (B) and 900 MHz for spectra (C) and (D). (A) Protiated ^{15}N labeled NAL single crystal at an arbitrary orientation. (B) Perdeuterated ^{15}N labeled NAL single crystal at an arbitrary orientation. (C) Uniformly ^{15}N labeled Pf1 coat protein in DMPC: Triton X-100 $q = 5$ bicelles. (D) Uniformly ^{2}H and ^{15}N labeled Pf1 coat protein (^{1}H back-exchanged) in DMPC: Triton X-100 $q = 5$ bicelles. (C) and (D) were oriented with their bilayer normals perpendicular to the direction of the magnetic field. Spectrum (B) was acquired with 20 kHz ^{2}H SPINAL-16 decoupling and spectrum (D) was acquired with 10 kHz ^{2}H SPINAL-16 decoupling. Spectral slices through the marked resonances are shown on the right side of the two-dimensional spectra. The line-widths in the ^{1}H-^{15}N heteronuclear dipolar coupling frequency dimension are 2.2 kHz for (A) and 0.85 kHz for (B).

Fig. 8.
Effects of perdeuteration on selected ^{1}H-^{15}N cross-polarization buildup curves. The ^{1}H resonance frequency was 700 MHz for spectra (A) and (B) and 900 MHz for spectra (C) and (D). (A) Protiated ^{15}N labeled NAL single crystal. (B) Perdeuterated ^{15}N labeled NAL single crystal. (C) Uniformly ^{15}N labeled Pf1 coat protein in DMPC: Triton X-100 $q = 5$ bicelles. (D) Uniformly ^{2}H and ^{15}N labeled Pf1 coat protein (^{1}H back-exchanged) in DMPC: Triton X-100 $q = 5$ bicelles. (C) and (D) were oriented with their bilayer normals perpendicular to the direction of the magnetic field. (A) and (B) were acquired with 20 kHz ^{2}H SPINAL-16 decoupling and (C) and (D) were acquired with 10 kHz ^{2}H SPINAL-16 decoupling.
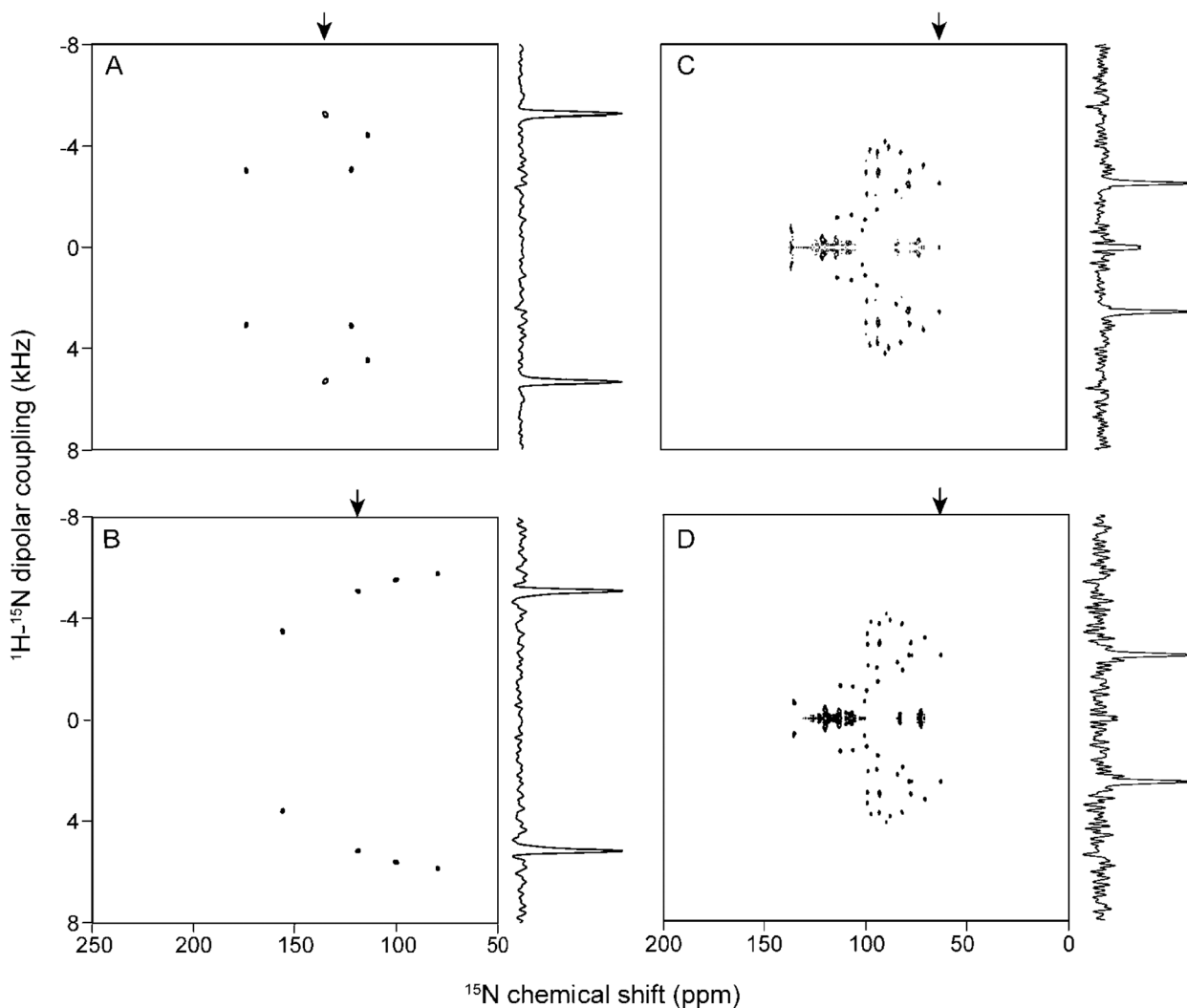
Fig. 9.
Effects of perdeuteration on two-dimensional SAMPI4 spectra. The ^{1}H resonance frequency
was 700 MHz for spectra (A) and (B) and 900 MHz for spectra (C) and (D). (A) Protiated
[15]N labeled NAL single crystal. (B) Perdeuterated ^{15}N labeled NAL single crystal. (C)
Uniformly ^{15}N labeled Pf1 coat protein in DMPC: Triton X-100 $q = 5$ bicelles. (D)
Uniformly ^{2}H and ^{15}N labeled Pf1 coat protein (^{1}H back-exchanged) in DMPC: Triton
X-100 $q = 5$ bicelles. The samples in (C) and (D) were oriented with their bilayer normals
perpendicular to the direction of the magnetic field. Spectrum (B) was acquired with 20 kHz
[2]H SPINAL-16 decoupling and spectrum (D) was acquired with 10 kHz ^{2}H SPINAL-16
decoupling. Representative spectral slices at the marked [1]H-^{15}N heteronuclear dipolar
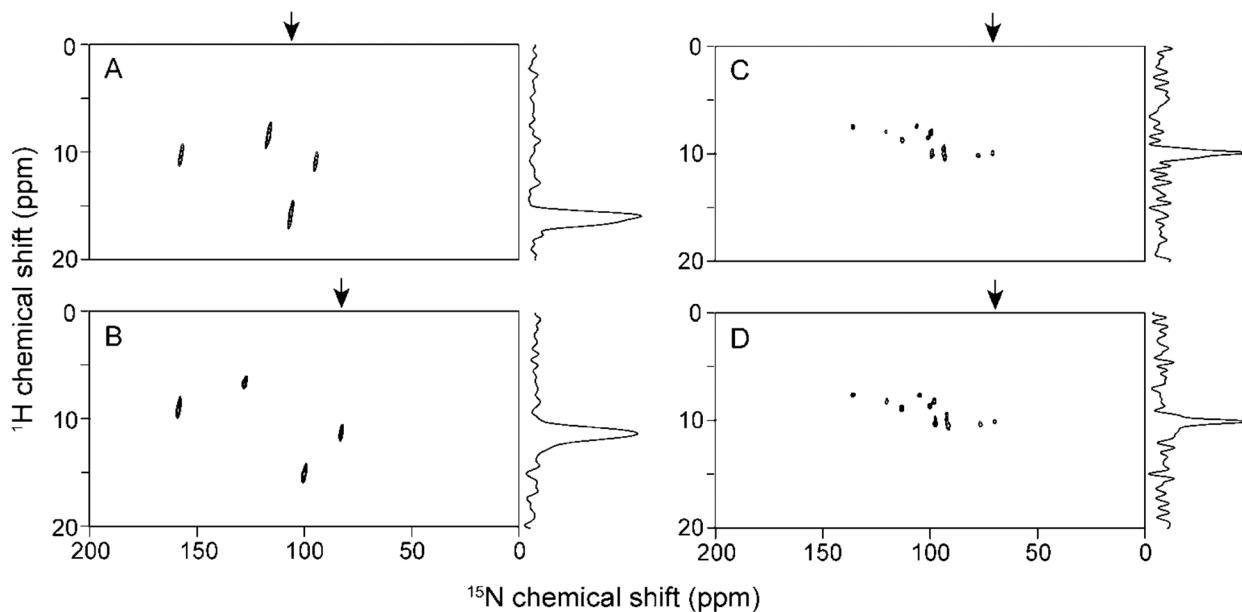coupling frequencies are shown on the right side of the spectra.

Fig. 10.
Effects of perdeuteration on two-dimensional ^{1}H-^{15}N heteronuclear correlation (HETCOR) experiments. The ^{1}H resonance frequency was 700 MHz for (A) and (B) and 900 MHz for (C) and (D). (A) Protiated ^{15}N labeled NAL single crystal. (B) Perdeuterated ^{15}N labeled NAL crystal. (C) Uniformly ^{15}N labeled Pf1 coat protein in DMPC: Triton X-100 $q = 5$ bicelles. (D) Uniformly ^{2}H and ^{15}N labeled Pf1 coat protein (^{1}H back-exchanged) in DMPC: Triton X-100 $q = 5$ bicelles. Samples used in (C) and (D) were oriented with the bilayer normals perpendicular to the direction of the magnetic field. The spectrum in (B) was acquired with 20 kHz ^{2}H SPINAL-16 decoupling and the spectrum in (D) was acquired with 10 kHz of ^{2}H SPINAL-16 decoupling. Spectra in (A) and (B) were acquired with 70 kHz ^{1}H power during t_1 while spectra (C) and (D) were acquired with 43 kHz ^{1}H power. Selected spectral slices in the ^{1}H chemical shift dimension are shown on the right side of the two-dimensional spectra.
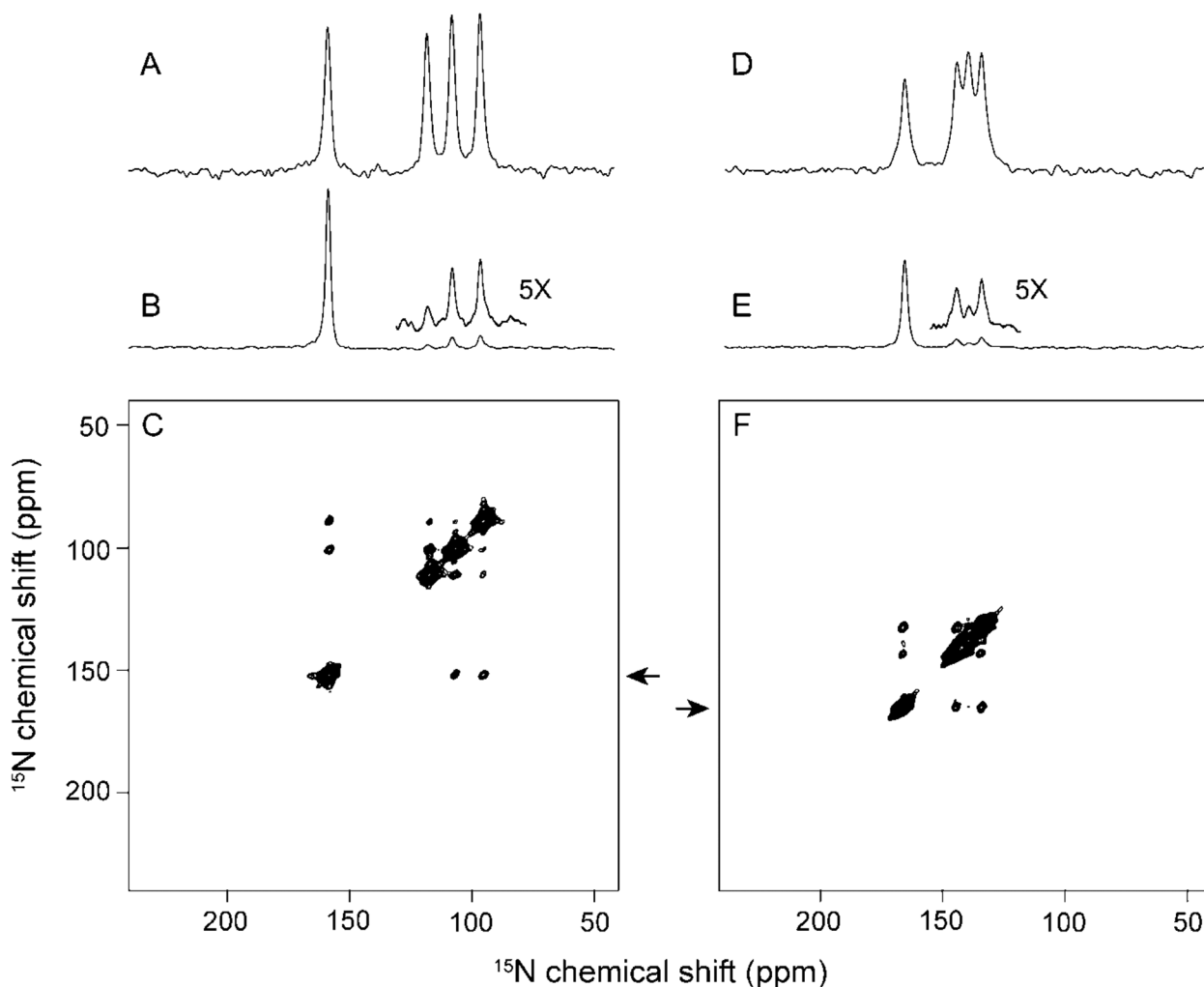
Fig. 11.
Effects of perdeuteration on two-dimensional PDSD spectra. The ^{1}H resonance frequency was 700 MHz. (A) - (C) Spectra of protiated ^{15}N labeled NAL single crystal. (D) - (F) Spectra of the perdeuterated ^{15}N labeled NAL single crystal. (A) and (D) are one-dimensional CP spectra of single crystals in which four distinct signals demonstrate that there are four unique molecules in each unit cell of the crystal. Spectrum in (B) is a slice through the spectrum in (C) taken at the marked frequency. 5X vertically expanded cross-peaks are shown above the slice. (C) is the PDSD spectrum of the protiated ^{15}N labeled NAL single crystal obtained with a 10 sec mix time. (E) is a slice through the spectrum in (F) at the marked frequency. The vertically expanded cross-peaks are shown above the slice. (F) is the PDSD spectrum of the perdeuterated labeled single crystal with a 10 sec mix time. Spectra in (C) and (F) are processed with 100 Hz of exponential line broadening in the F1 and F2 frequency dimensions. Both the one and two-dimensional spectra resulted from signal averaging 32 scans.
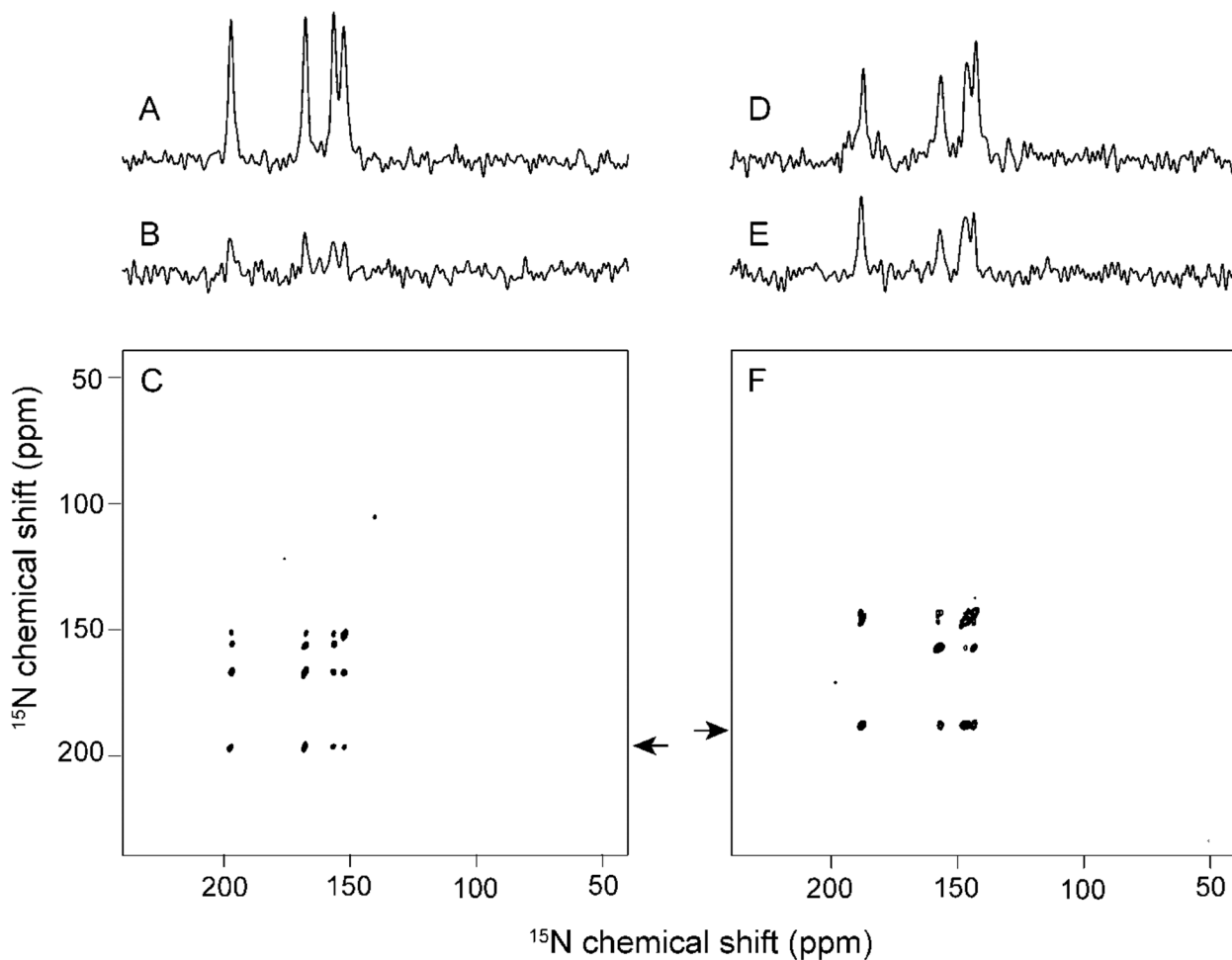
Fig. 12.
Effects of perdeuteration on two-dimensional MMHH spectra. The ^{1}H resonance frequency was 700 MHz. (A) is a one-dimensional CP spectrum of a protiatated ^{15}N labeled NAL single crystal. (D) is a one-dimensional CP spectrum of a perdeuterated ^{15}N labeled NAL single crystal. (C) is an MMHH spectrum from a protiated ^{15}N labeled NAL single crystal. (F) is an MMHH spectrum from a perdeuterated ^{15}N labeled NAL single crystal. (B) is a one-dimensional slice through spectrum (C) taken at the marked position. The spectrum (C) was acquired with 10 msec MMHH pulse at a 15% mis-match level. (E) is a one-dimensional slice taken at the marked position through spectrum (F). The MMHH experiment on a perdeuterated ^{15}N labeled NAL single crystal was performed with a 10 msec MMHH pulse at a 5% mis-match level. Spectra (C) and (F) were both processed with 40 Hz line broadening in the F2 dimension (horizontal) and 100 Hz line broadening in the F1 dimension (vertical). The one-dimensional spectra were obtained with 4 scans and the two-dimensional ^{15}N labeled NAL single crystal spectra were obtained with 32 scans.
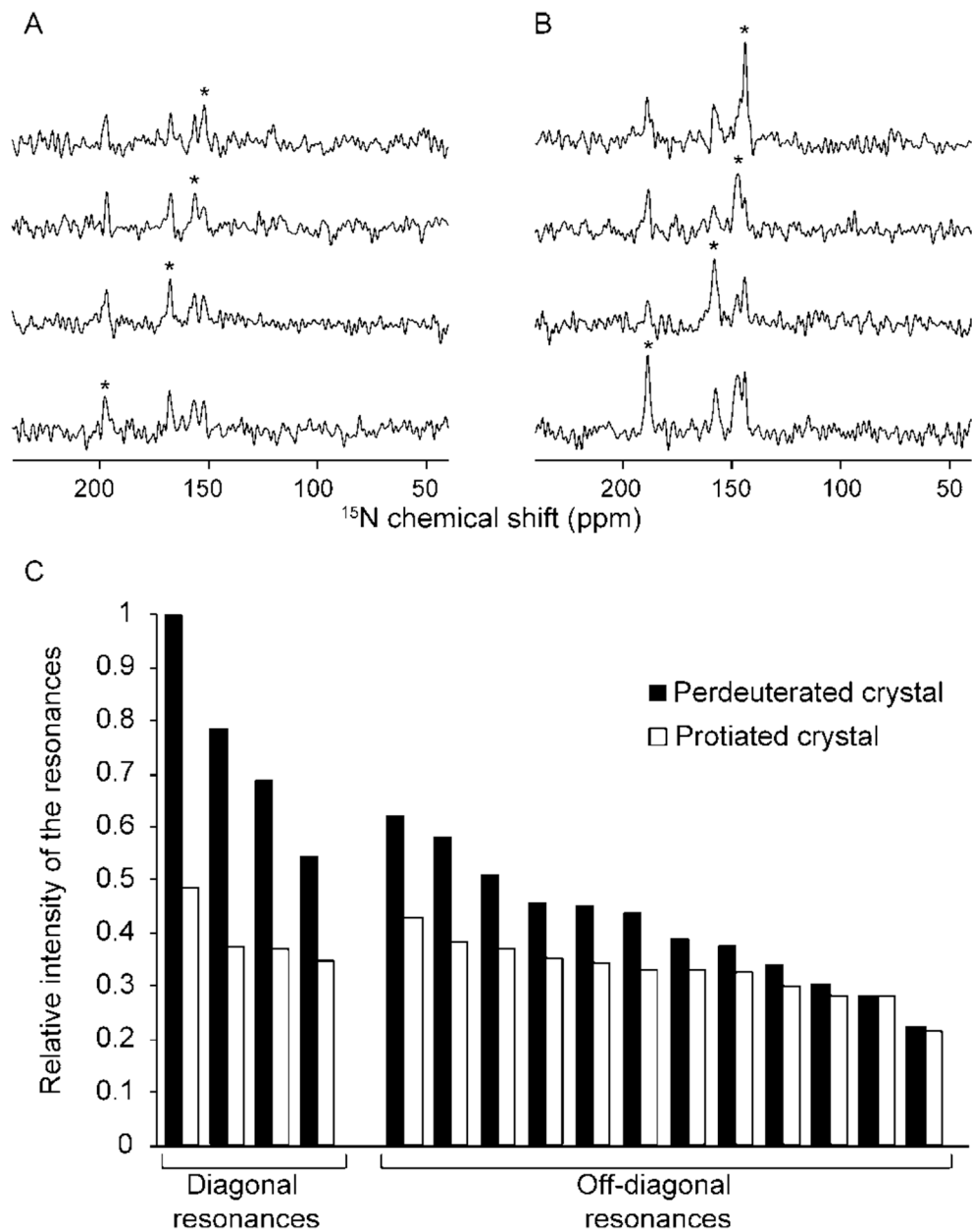
Fig. 13.
One-dimensional slices through each diagonal peak from the two-dimensional Mismatched Hartmann-Hahn (MMHH) experiments (Fig. 12) for the protiated (A) and perdeuterated (B) NAL crystals. Asterisks indicate the position of the diagonal peaks. (C) Relative experimental intensity of the on- and off-diagonal resonances ranked in high to low order are shown from left to right. Black columns represents the values in the perdeuterated crystal, and white columns represents the values for the protiated crystal. Normalization was performed based on the largest intensity value across the two spectra.

Table 1

Capacitance values used in the (A) 700 MHz and (C) 900 MHz probes. The circuit diagrams are depicted in Fig. 1. The performance data for (B) 700 MHz and (D) 900 MHz using typical power levels.

A

700 MHz triple resonance HDN probe

Label	C1	C4	C5	C6	C7	C8	C11
Value(pf)	10	0.75	33	3.3	68	5.6	48

B

700 MHz triple resonance HDN probe

Nucleus	Power (W)	B_1 (kHz)
^1H	50	115
^2H	250	52.6
^{15}N	300	56.8

C

900 MHz triple resonance HDN probe

Label	C1	C4	C5	C6	C8	C9	C10	C11	C12	C15	C16
Value(pf)	5.6	1.1	2.2	1.1	15	3.9	1.5	3.9	18	39	27

D

900 MHz triple resonance HDN probe

Nucleus	Power (W)	B_1 (kHz)
^1H	200	51.5
^2H	80	20
^{15}N	400	46.3